ADVANCED MATERIALS
www.advmat.de

Fully Printed, High-Temperature Micro-Supercapacitor Arrays Enabled by a Hexagonal Boron Nitride Ionogel Electrolyte

*Lindsay E. Chaney, Woo Jin Hyun, Maryam Khalaj, Janan Hui, and Mark C. Hersam**

The proliferation and miniaturization of portable electronics require energy-storage devices that are simultaneously compact, flexible, and amenable to scalable manufacturing. In this work, mechanically flexible micro-supercapacitor arrays are demonstrated via sequential high-speed screen printing of conductive graphene electrodes and a high-temperature hexagonal boron nitride (hBN) ionogel electrolyte. By combining the superlative dielectric properties of 2D hBN with the high ionic conductivity of ionic liquids, the resulting hBN ionogel electrolyte enables micro-supercapacitors with exceptional areal capacitances that approach 1 mF cm^{-2}. Unlike incumbent polymer-based electrolytes, the high-temperature stability of the hBN ionogel electrolyte implies that the printed micro-supercapacitors can be operated at unprecedentedly high temperatures up to 180 °C. These elevated operating temperatures result in increased power densities that make these printed micro-supercapacitors particularly promising for applications in harsh environments such as underground exploration, aviation, and electric vehicles. The combination of enhanced functionality in extreme conditions and high-speed production via scalable additive manufacturing significantly broadens the technological phase space for on-chip energy storage.

1. Introduction

The rising demand for portable electronics is driving the need for innovative on-chip energy-storage solutions. For example, the expanding Internet of Things (IoT) requires widespread, self-powered sensor networks that are robust in diverse environmental conditions. For remote and autonomous operation, these devices rely on compact, integrated power sources.[1–3] Micro-supercapacitors (MSCs) are promising power sources for distributed sensor networks due to their exceptionally long cycle lives coupled with rapid energy delivery and uptake.[4] Additionally, the MSC planar device architecture is easily integrated with all components of a wireless sensor, allowing for streamlined manufacturing directly on a single substrate.[5]

Supercapacitors store energy via the formation of an electrochemical double layer at the electrode–electrolyte interface. Since the ion adsorption and desorption process is rapid and fully reversible, supercapacitors possess higher power densities and significantly longer cycle lives compared to batteries.[6,7] Because the strengths of supercapacitors complement the relatively high energy densities of batteries, these two technologies are often used in tandem as a comprehensive energy-storage solution.[8] Moreover, the rapid charging capabilities of supercapacitors make them ideal to be integrated with remote energy harvesters[1] or wireless charging coils.[9]

Planar MSCs consist of both positive and negative electrodes on a single substrate, often in an interdigitated electrode (IDE) geometry. This architecture is attractive for on-chip integrated energy storage because the power source can be fabricated alongside other device components instead of as a bulky addition. Conventional microfabrication techniques (e.g., photolithography) can be used to pattern IDEs with exceptionally small features.[10] However, these techniques are neither

L. E. Chaney, W. J. Hyun, M. Khalaj, M. C. Hersam
Department of Materials Science and Engineering
Northwestern University
Evanston, IL 60208, USA
E-mail: m-hersam@northwestern.edu

The ORCID identification number(s) for the author(s) of this article can be found under https://doi.org/10.1002/adma.202305161

DOI: 10.1002/adma.202305161

W. J. Hyun
Department of Materials Science and Engineering
Guangdong Technion–Israel Institute of Technology
Shantou, Guangdong 515063, China

J. Hui, M. C. Hersam
Department of Chemistry
Northwestern University
Evanston, IL 60208, USA

M. C. Hersam
Department of Medicine
Department of Electrical and Computer Engineering
Northwestern University
Evanston, IL 60208, USA

generally compatible with flexible or wearable devices, nor are they well poised for industrial manufacturing due to the necessity of clean room processing and toxic chemicals.[11] Similarly, other lab-scale fabrication techniques that are typically employed in thin-film energy-storage research, such as physical and chemical vapor deposition, spin coating, and spray coating, are absent from industrial energy-storage manufacturing due to their low throughput.[12,13] Therefore, the on-chip energy-storage sector stands to benefit greatly from alternative scalable fabrication methods.

Due to their low waste and rapid deposition of electronic materials, additive manufacturing methods hold significant promise in this context. Among additive manufacturing options, screen printing is particularly desirable due to its high throughput and proven utility for electronics manufacturing such as printed circuit boards.[14,15] During screen printing, a viscous ink is pushed through a prepatterned mesh screen using a squeegee and deposited onto a substrate. Unlike related deposition methods (e.g., blade coating), screen printing can form complex patterns at the microscale. In addition, multistep screen printing enables layer-by-layer deposition of each electrically active component for streamlined fabrication of integrated planar microdevices with high reproducibility.

Among printed electronic materials, graphene is particularly attractive as a supercapacitor electrode material because of its large specific surface area, high electrical conductivity, exceptional theoretical capacitance, and robust mechanical properties.[16] Furthermore, graphene nanoplatelets can be scalability produced and dispersed in various solvents via liquid-phase exfoliation. For these reasons, graphene is widely used as a printable electrode material in thin-film transistors and energy-storage devices.[17–21] On the other hand, relatively little effort has been focused on printable solid-state electrolytes. While some examples exist,[22–24] a large-scale, high-throughput printed solid-state electrolyte has not yet been established for MSCs. For example, while inkjet-printed MSC arrays have been produced using graphene IDEs and polymer electrolytes,[22] the manufacturing scalability of this approach is limited by the inherently low throughput of drop-on-demand methods like inkjet printing. Furthermore, these inkjet-printed MSC arrays require 20 total printing passes to achieve the optimal electrolyte print thicknesses due to the low ink deposition volume. In contrast, contact printing methods like screen printing have throughputs that are orders of magnitude higher than drop-on-demand methods.[25] Meanwhile, other attempts to employ additive manufacturing methods for supercapacitors have not printed every component including the current collector and electrolyte, limiting their ultimate scalability.[26–29] Therefore, the development of suitable inks for high-throughput, multistep additive manufacturing remains an unmet yet critical need for MSCs.

Here, we present the inks and methodology for achieving rapid manufacturing of MSCs in which all electrochemically active components are screen-printed. The key innovation is a screen-printable ionogel electrolyte consisting of hexagonal boron nitride (hBN) nanoplatelets and 1-ethyl-3-methylimidazolium bis(trifluoromethylsulfonyl)imide (EMIM-TFSI) ionic liquid that is fully compatible with pre-screen-printed graphene IDEs. This hBN ionogel was first reported as an electrolyte for Li-ion batteries,[30] and subsequent reports have focused on alternative deposition methods for batteries and thin-film transistors.[31,32] In contrast, this work reports the first demonstration of rapid, precise, and large-area patterning of the hBN ionogel for integrated supercapacitor arrays.

Unlike incumbent polymer-based electrolytes, the hBN ionogel is stable in extreme conditions including at high temperatures up to 180 °C. This stability holds promise for self-powered IoT devices that can be deployed in harsh environments such as underground exploration,[33,34] aviation,[35] and electric vehicles[36,37] for expanded sensing capabilities. Moreover, a high-temperature energy-storage solution eliminates the need for bulky cooling systems or temperature-resistant cables to transmit information.[35] By addressing the challenges of high-temperature electronics directly from a materials engineering perspective, we demonstrate an energy-storage methodology that can inherently run at high temperature rather than relying on extrinsic cooling solutions.

In addition to achieving superlative areal capacitances that approach 1 mF cm^{-2}, these MSCs can be directly and rapidly printed in series and parallel configurations to allow full control over the voltage and power outputs that are needed for diverse technological requirements. In this manner, this work represents a significant step forward toward scalable manufacturing of on-chip energy storage, particularly for applications in extreme environments.

2. Results and Discussion

2.1. Screen-Printable Hexagonal Boron Nitride Ionogel Ink

Rapidly printed, high-temperature MSCs are enabled by a screen-printable hBN ionogel electrolyte ink (**Figure 1**). The electrolyte consists of the ionic liquid EMIM-TFSI and a gelling matrix of exfoliated hBN nanoplatelets (Figure 1a). When combined, a stiff electrolyte gel is formed (Figure 1b) with an ionic conductivity of ≈5 mS cm^{-1} (Figure 1c) and a storage modulus of ≈4 MPa (Figure 1d) at room temperature. The hBN nanoplatelets are produced via a scalable liquid-phase exfoliation process that has been reported previously.[31,32] The high-surface-area nanostructured hBN matrix of the ionogel increases interactions with the ionic liquid and leads to an exceptionally high mechanical modulus at sufficiently low hBN loadings that preserve high ionic conductivity.[30,38]

Screen printing requires highly viscous inks to produce high-resolution, high-fidelity printed features.[25] Thus, it is crucial to choose a compatible solvent that can disperse the hBN ionogel components at high concentrations. Simultaneously, screen-printable inks must exhibit shear thinning, meaning that they become significantly less viscous under applied shear stress from the squeegee but stiffen and retain their shape once the squeegee is removed.[39] Finally, high-boiling-point solvents need to be utilized in order to avoid mesh clogging from solvent evaporation between prints.[10] These ink requirements were met through careful formulation of the screen-printable hBN ionogel ink. Specifically, the viscosity of the ink was tuned to be compatible with high-throughput screen printing by varying the concentration of the hBN ionogel components in the nontoxic, high-boiling-point solvent ethyl lactate (EL). The optimized screen-printable ink formulation consists of a 1:2:2 mass ratio of hBN

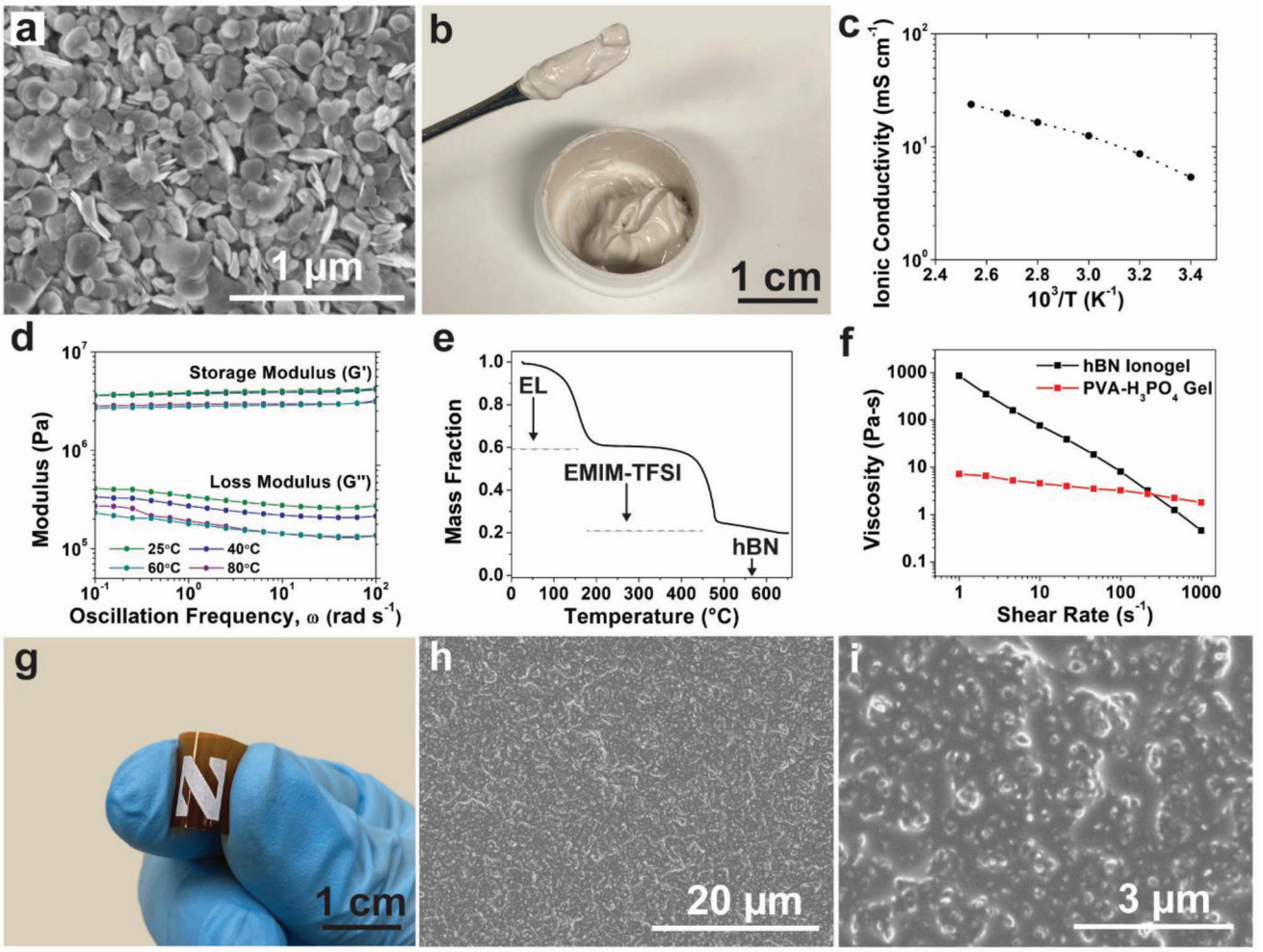

Figure 1. Exfoliated hBN ionogel screen-printable ink. a) SEM image of exfoliated hBN nanoplatelets. b) Photograph of the hBN ionogel screen-printable ink. c) Ionic conductivity as a function of temperature for the hBN ionogel. The dashed line is a Vogel–Fulcher–Tammann (VFT) model fit. d) Temperature dependence of the storage and loss moduli of the hBN ionogel. e) Thermogravimetric analysis of the hBN ionogel screen-printable ink, which indicates that the ink composition is 1:2:2 of hBN:EMIM-TFSI:ethyl lactate by mass. f) Viscosity as a function of shear rate of the hBN ionogel ink and a PVA–H_3PO_4 gel. g) Photograph of a screen-printed ionogel feature on a flexible polyimide substrate. h,i) SEM images of the printed hBN ionogel at two different magnifications.

nanoplatelets:EMIM-TFSI ionic liquid:EL (Figure 1e). This formulation produces a shear-thinning ink with a viscosity of 76 Pa s at a shear rate of 10 s^{-1} (Figure 1f). Ultimately, the stiffness imparted by the nanostructured hBN ionogel matrix leads to a viscous ink without the use of additives that could disrupt ion conduction in the electrolyte film. Following ink formulation, the hBN ionogel was deposited using an automated screen printer, resulting in a homogeneous film (Figure 1g). The relatively low volatility of the EL enabled continuous printing without mesh clogging issues. Scanning electron microscopy (SEM) images of the printed hBN ionogel show that the hBN nanoplatelets are well distributed within the ionic liquid (Figure 1h,i). The thickness of the film was measured by laser confocal microscopy and determined to be 14.0 ± 0.3 μm with a root-mean-square roughness of 2.2 μm.

Currently, gel electrolytes based on polyvinyl alcohol (PVA) and H_3PO_4 are widely used for graphene-based solid-state supercapacitors.[40,41] However, PVA–H_3PO_4 gel electrolytes are inherently ill-suited for screen printing since they show limited shear-thinning behavior (Figure 1f) and produce rough, nonuniform films. In addition, the acid component of PVA–H_3PO_4 gel electrolytes corrodes stainless-steel mesh screens when employed continuously for large-scale manufacturing. While there have been rare instances of screen-printable polymer-based MSC electrolytes,[23,24] these studies have been limited to single device demonstrations and contain no discussion of print quality or scalability. In contrast, our screen-printable hBN ionogel electrolyte enables reliable patterning that routinely produces hundreds of devices. Furthermore, our hBN–ionogel-based MSCs achieve areal capacitances approaching 1 mF cm^{-2}, which meet or exceed the areal capacitance of previously reported graphene MSCs based on polymer electrolytes (Table S1, Supporting Information).

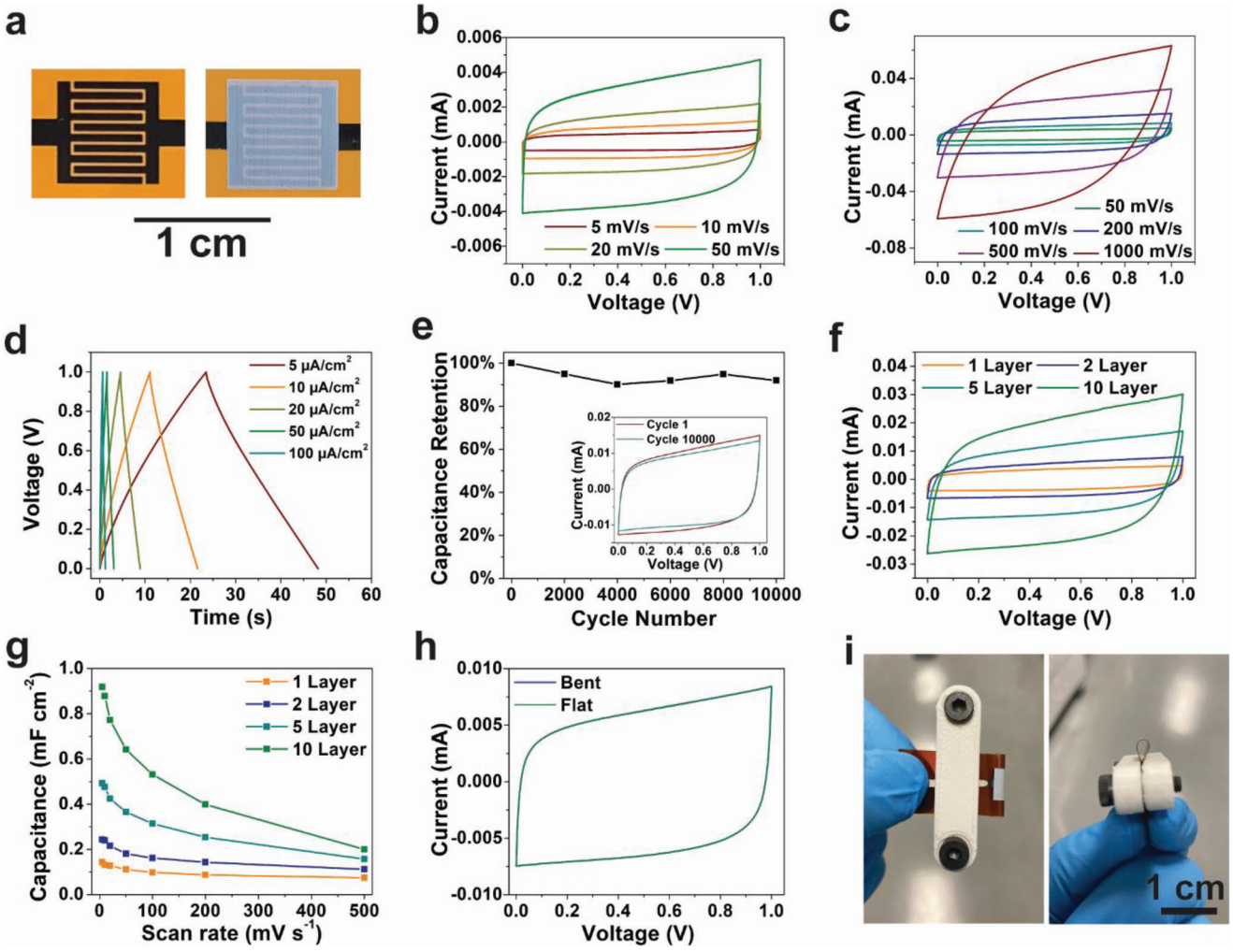

Figure 2. Electrochemical performance of the fully printed micro-supercapacitor device. a) Left: photograph of the graphene interdigitated electrodes; right: completed device with the hBN ionogel printed on top of the graphene interdigitated electrodes. b,c) Cyclic voltammograms of a single micro-supercapacitor device at low and high scan rates. d) Galvanostatic charge–discharge curves for a single micro-supercapacitor device. e) Capacitance as a function of cycle number for a single micro-supercapacitor device. Inset: cyclic voltammograms at cycles 1 and 10 000. f) Cyclic voltammograms for micro-supercapacitor devices printed with 1, 2, 5, and 10 layers of graphene (scan rate: 50 mV s^{-1}). g) Rate capability of micro-supercapacitor devices printed with 1, 2, 5, and 10 layers of graphene. h) Cyclic voltammograms of a single micro-supercapacitor device during bending (bending radius: 1.5 mm; scan rate: 50 mV s^{-1}). i) Photographs of a micro-supercapacitor device during bending tests.

2.2. Micro-Supercapacitor Device Fabrication and Characterization

Figure 2 delineates the electrochemical performance of our MSC devices. All electrochemically active components were screen-printed, including the graphene IDEs and the hBN ionogel electrolyte (Figure 2a). The screen-printable graphene ink is adapted from a previous formulation[42] and is composed of a composite of graphene nanoplatelets and ethyl cellulose dispersed in terpineol. The composition and rheological properties of the screen-printable graphene ink are described in Figure S1a,b (Supporting Information). The screen-printed graphene IDEs have a total geometric area of 0.56 cm^2 with a finger width of 540 μm and a gap width of 250 μm (Figure S1c, Supporting Information). Following screen printing, the graphene electrodes are cured at 350 °C for 30 min to remove ethyl cellulose. The resulting screen-printed electrodes consist of a high-quality percolating network of graphene flakes (Figure S1d, Supporting Information) with an electrical conductivity of ≈4 ×10^4 S m^{-1}. Figure S2 (Supporting Information) shows photographs of the patterned mesh screens, and Figure S3 (Supporting Information) provides further electrical and mechanical characterization of the graphene films. Each graphene printed layer is ≈690 nm thick, and the overall graphene film thickness increases almost linearly as additional layers are deposited via screen printing. Due to the exceptionally high electrical conductivity of the graphene electrodes, no current collector was required, eliminating this common fabrication step. The hBN ionogel was then screen-printed on top of the graphene IDEs and dried at 160 °C for 30 min to remove residual EL. A video depicting the hBN ionogel printing process is shown in Video S1 (Supporting Information).

The MSC devices were electrochemically characterized using cyclic voltammetry (CV) and galvanostatic measurements. Rectangular cyclic voltammograms absent of redox peaks (Figure 2b,c) along with triangular galvanostatic charge–discharge curves (Figure 2d) indicate ideal electrochemical double-layer behavior even at high discharge rates. The 1 V voltage window was chosen to avoid deviations from ideal behavior at larger applied voltages, likely due to the presence of water in the hygroscopic ionogel (Figure S4, Supporting Information). The MSC devices also display a capacitance retention of 91.9% after 10 000 charge–discharge cycles (Figure 2e). The active material loading was adjusted by increasing the number of printed graphene layers, leading to larger capacitance values (Figure 2f,g). An areal capacitance of 0.14 mF cm^{-2} was achieved with a single graphene print layer, while 0.92 mF cm^{-2} was achieved with ten print layers (an electrode thickness of ≈7.5 µm). The Supporting Information contains details of the capacitance calculations, and Table S2 (Supporting Information) summarizes the performance metrics for the devices, including areal capacitance, energy density, and power density. A Ragone plot comparing the performance of devices with different thicknesses is also provided in Figure S5 (Supporting Information). Finally, Figure S6 (Supporting Information) shows electrochemical impedance spectroscopy (EIS) data for various devices and operating conditions with Table S3 (Supporting Information) summarizing the EIS fitting parameters.

Traditional sandwich-structured devices typically do not benefit from higher active material loadings because the counter ions must penetrate deeper into the electrode films. However, an advantage of the interdigitated electrode geometry is that ions penetrate laterally into the graphene film, enabling low-barrier access to the space between individual graphene sheets, thus effectively increasing the electroactive surface area.[43,44] As shown in Table S1 (Supporting Information), the capacitance of our hBN ionogel-based MSCs compares favorably with other recent graphene MSC demonstrations, all of which use incumbent polymer-based electrolytes. Furthermore, polymer-based electrolytes are known to suffer from solvent evaporation or degradation of the polymer host by the acid over time, which leads to decreased ionic conductivity and performance.[22,40,45] In contrast, the hBN ionogel devices were tested 15 months after the original fabrication and were shown to have almost identical performance (Figure S7, Supporting Information).

Since 2D materials are intrinsically flexible, the screen-printed MSCs can also withstand mechanical flexing. In particular, full capacitance is maintained while flexing the MSCs to a 1.5 mm bending radius (Figure 2h,i) and after 500 bending cycles (Figure S8, Supporting Information). This mechanical resilience is enabled by the highly flexible graphene electrodes and the gel-like behavior of the hBN electrolyte. It is noteworthy that the carefully selected diluent solvent EL results in crack-free screen-printed films after its thermal removal. Thus, the uninterrupted ion-diffusion path throughout the entire device leads to excellent electrochemical performance in addition to reinforcing high mechanical integrity and flexibility. In contrast to traditional sandwich-structured supercapacitors, the interdigitated electrode architecture of these MSC devices also eliminates the risk of leakage or device shorting.

2.3. Micro-Supercapacitor Device Integration

In order to meet a wide range of voltage and current requirements, the individual MSCs can be integrated to form series and/or parallel device arrays (**Figure 3**). For example, high-voltage power supplies are commonly required for various portable electronics such as microrobotics, microsensors, and soft actuators.[22,29,46,47] Due to the high electrical conductivity of the screen-printed graphene films, the same graphene ink is used to screen-print the conductive interconnects. Various integrated device configurations are shown, including two devices in series (2S), two devices in parallel (2P), and a 2S×2P array of devices (Figure 3a). Corresponding cyclic voltammograms and galvanostatic charge–discharge curves show expected outputs—namely, two devices connected in series expand the operating voltage window, while two devices connected in parallel result in increased discharge current (Figure 3b,c). Unlike drop-on-demand printing methods, screen printing can rapidly pattern large-area device arrays. For example, 100 devices (10S × 10P) are patterned with negligible additional effort compared to a single device (Figure 3d). These arrays maintain excellent electrochemical performance, displaying rectangular cyclic voltammograms and triangular galvanostatic curves in the extended 10 V window (Figure 3e,f). The 10S × 10P array also maintains resilience to mechanical flexing, as its performance is unaffected when it is operated under a bending radius of 2.5 cm (Figure 3g,h).

2.4. Micro-Supercapacitor High-Temperature Operation

Traditional supercapacitors suffer from a number of failure mechanisms at high temperature, which mainly stem from insufficient thermal stability of device components and loss of the ion-conducting medium.[48] Liquid electrolytes become volatile and flammable at increased temperatures, and even solid polymer-based electrolytes begin to dry and degrade by 100 °C. On the other hand, the hBN ionogel can withstand high temperatures without degradation due to the use of an ionic liquid. The screen-printed device performance at elevated temperatures is summarized in **Figure 4**. Cyclic voltammograms of a single device display near-rectangular behavior up to 180 °C (Figure 4a). Because the viscosity of the electrolyte decreases at elevated temperatures, the ionic conductivity increases and leads to improved capacitance.[40,49] The reduced electrolyte viscosity also allows the electrolyte ions to more easily penetrate the graphene film and access the nanostructured surface of the electrodes.[34,50,51] While higher temperature enhances performance for these reasons, it can also lead to challenges including faster electrolyte degradation and increased side reactions between the electrolyte and the active material.[50] When these factors become dominant, the practical temperature limit for stable device operation is reached. Some distortion of the cyclic voltammograms and a plateau in the power output begin to occur above 180 °C, likely due to side reactions. For these reasons, 180 °C was deemed to be the maximum practical operating temperature even though the devices could be cycled at higher temperatures without issues (Figure S9, Supporting Information). Cycle life testing shows that

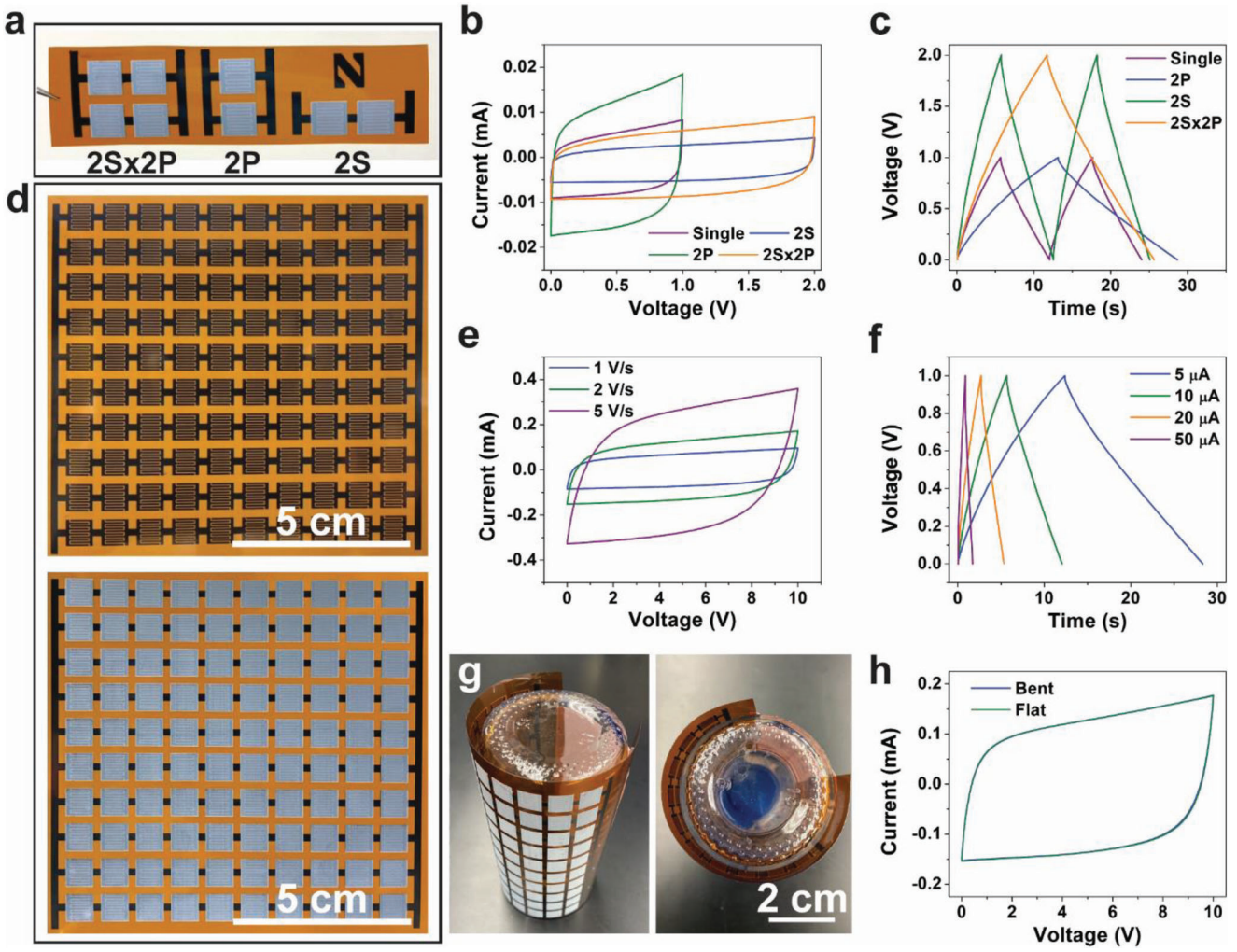

Figure 3. Micro-supercapacitor device integration. a) Photograph of small-scale integrated device configurations: two devices in series (2S), two devices in parallel (2P), and a 2×2 array of devices (2S×2P). b) Cyclic voltammograms of various micro-supercapacitor device configurations (scan rate: 100 mV s^{-1}). c) Galvanostatic charge–discharge curves of various micro-supercapacitor device configurations (applied current: 10 μA). d) Top: photograph of a 10S×10P array of screen-printed graphene interdigitated electrodes before the hBN ionogel was printed; bottom: photograph of a fully printed 10S×10P micro-supercapacitor array consisting of the hBN ionogel printed on top of the graphene interdigitated electrodes. e) Cyclic voltammograms of the 10S×10P micro-supercapacitor array. f) Galvanostatic charge–discharge curves of the 10S×10P micro-supercapacitor array. g) Photographs of the 10S×10P micro-supercapacitor array while being flexed around a 2.5 cm bending radius. h) Cyclic voltammograms of the 10S×10P micro-supercapacitor array, showing indistinguishable performance while in the bent and flat orientations (scan rate: 2 V s^{-1}).

the devices retain 93.6% capacitance after 1000 charge–discharge cycles at 180 °C (Figure 4b). The 10S × 10P array also displays excellent cycling behavior at elevated temperatures, including increased capacitance (Figure 4c) and a power output of 2.6 mW at 180 °C (Figure 4d). Figure S10 (Supporting Information) shows a demonstration of a 10S×10P array powering a digital clock display while being exposed to 180 °C. In contrast to common polymer-based electrolytes (e.g., PVA–H_3PO_4) that begin to degrade at ≈100 °C and show visible cracking at 180 °C,[35] the hBN ionogel shows no sign of degradation at these temperatures (Figure 4e) and can continue to be cycled even after exposure to 300 °C (Figure S11, Supporting Information). Consequently, the screen-printed hBN ionogel opens up unprecedented opportunities for on-chip remote power sources in extreme environments.

3. Conclusion

We have demonstrated fully and rapidly screen-printed MSC arrays based on a high-temperature hBN ionogel electrolyte with robust mechanical properties and state-of-the-art ionic conductivity. Importantly, the device fabrication is entirely based on screen printing, which is a high-throughput additive manufacturing method that is widely used in printed electronics manufacturing. Moreover, this fabrication strategy minimizes waste, making it both scalable and environmentally sustainable. Exceptional areal capacitances approaching 1 mF cm^{-2} are achieved with the combination of screen-printed graphene IDEs and the hBN ionogel. By employing hBN as the solid matrix, we entirely replace the polymers that limit high-temperature performance in incumbent gel electrolytes. As a result, the screen-printed

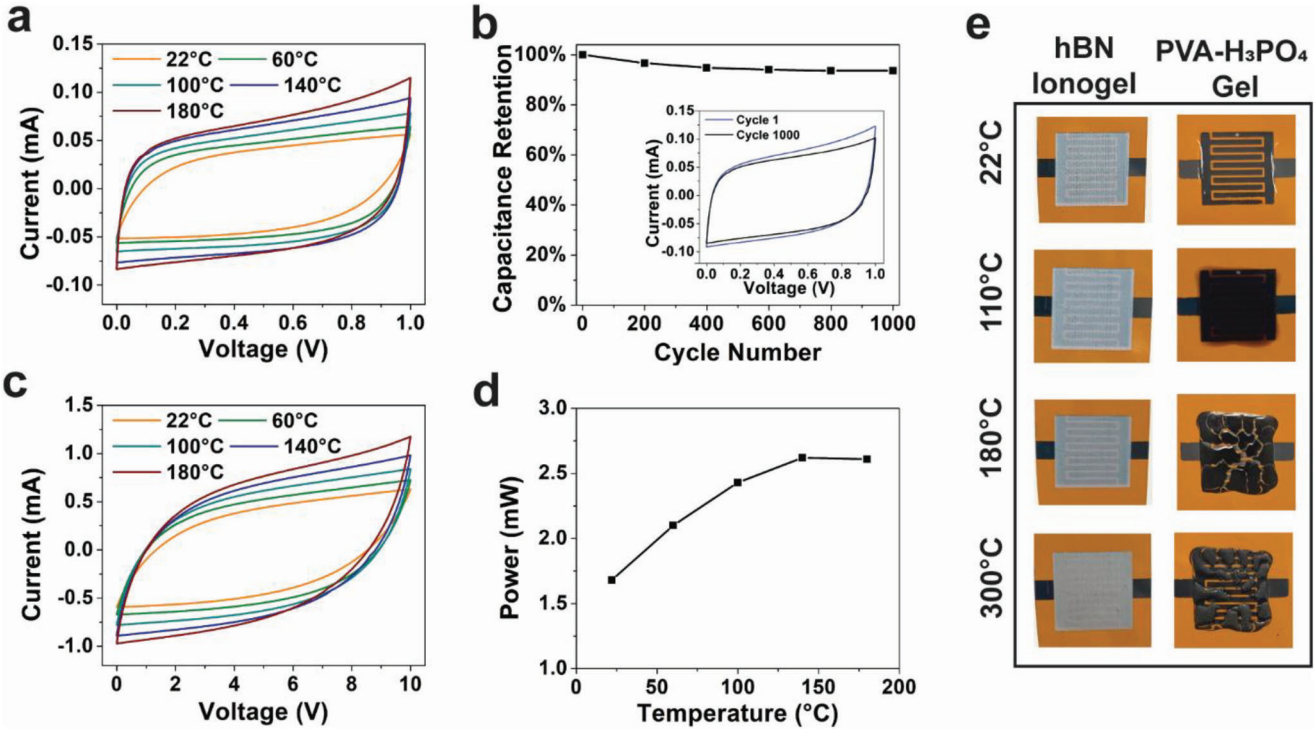

Figure 4. High-temperature operation of screen-printed micro-supercapacitors. a) Cyclic voltammograms of a single micro-supercapacitor device at elevated operating temperatures (scan rate: 1 V s^{-1}). b) Capacitance retention as a function of cycle number for a single micro-supercapacitor device operating at 180 °C (scan rate: 1 V s^{-1}). Inset: cyclic voltammograms at cycles 1 and 1000. c) Cyclic voltammograms of a 10S×10P array of micro-supercapacitor devices at elevated operating temperatures (scan rate: 10 V s^{-1}). d) Output power as a function of operating temperature of the 10S×10P micro-supercapacitor array. e) Comparative photographs of micro-supercapacitor devices based on the hBN ionogel electrolyte and a PVA–H_3PO_4 polymer gel electrolyte after exposure to elevated temperatures.

MSC arrays maintain excellent cyclability up to 180 °C with improved power density due to the increased ionic conductivity of the hBN ionogel electrolyte at elevated temperatures. Overall, this work establishes an additive manufacturing platform that can support future on-chip energy storage for extreme-environment applications in underground exploration, aviation, and electric vehicles.

4. Experimental Section

Ionogel Ink Formulation and Characterization: To produce the hBN nanoplatelets, 120 g of hBN powder (1 µm, Sigma–Aldrich), 12 g of ethyl cellulose (4 cp, Sigma–Aldrich), and 1 L of ethanol (200 proof, Decon Labs) were shear mixed for 2 h at 10 230 rpm (L5M-A, Silverson). The resulting dispersion was centrifuged at 4000 rpm for 20 min to remove unexfoliated material. The supernatant was collected and mixed with a 0.04 g mL^{-1} solution of aqueous sodium chloride and centrifuged at 7500 rpm for 7 min. The flocculated material was then rinsed, dried, and ground to form a powder. Finally, the resulting powder was baked in a box furnace at 400 °C for 4 h to remove the ethyl cellulose. To form the hBN ionogel ink, the exfoliated hBN powder was combined with EMIM-TFSI ionic liquid (≥98% (HPLC), Sigma–Aldrich) and ethyl lactate (Sigma–Aldrich) in a weight ratio of 1:2:2 and mixed in a centrifugal mixer (ARE-310, Thinky USA) with ceramic ball bearings for 20 min at a maximum speed of 2000 rpm. Thermogravimetric analysis was performed on a Mettler Toledo TGA/DSC 3+, and rheometry measurements were performed on an Anton Paar MCR 302. The viscoelastic properties of the hBN ionogel were measured using an 8 mm parallel plate geometry, a 1 mm gap, a shear strain of 0.1%, and an oscillation frequency range of 0.1–100 Hz. SEM images of the hBN nanoplatelets and the hBN ionogel were performed on a Hitachi SU8030 SEM after an osmium layer was deposited. The ionic conductivity (σ) of the hBN ionogel was measured using a coin cell configuration (CR2032) in which the ionogel was manually inserted between two stainless-steel disks. Equation (1) is used to determine the conductivity

$$\sigma = \frac{t}{R \times A} \tag{1}$$

where t is the thickness and A is the area of the hBN ionogel. R represents the bulk resistance, which was determined by EIS in a frequency window from 1 MHz to 1 Hz using a potentiostat (VSP, BioLogic). The temperature dependence of the ionic conductivity was determined in an environmental chamber (BTX-475, Espec) at 20, 40, 60, 80, 100, and 120 °C, sequentially. The experimental data were fitted to the Vogel–Fulcher–Tammann (VFT) model curve according to Equation (2)

$$\sigma = A \exp\left(-\frac{B}{T - T_0}\right) \tag{2}$$

with A, the pre-exponential factor, set at 125.51 mS cm^{-1}, B, the pseudoactivation energy term related to the entropic barrier to ion motion, set at 358.11 K^{-1}, and T_0, the ideal glass transition temperature, set at 179.32 K. Laser confocal microscopy thickness and roughness measurements were performed on an Olympus LEXT OLS5000 optical microscope fitted with a ×50 objective lens (numerical aperture = 0.95).

Device Fabrication and Characterization: The graphene screen-printable ink was prepared by mixing graphene–ethyl cellulose composite powder (reported previously)[52] with terpineol at 140 mg mL^{-1} using a centrifugal mixer (ARE-310, Thinky USA) and ceramic ball bearings

for 60 min at a maximum speed of 2000 rpm. The patterned screen employed 325-mesh stainless steel stretched over a 12×12 in. aluminum frame (Hary Manufacturing, Inc.). The screen printer (886 PC DSIV, Hary Manufacturing Inc.) was programmed with the following settings: squeegee and flood plate pressures of 20 psi, a speed of 127 mm s^{-1}, and a snapoff distance of 1016 µm. Following printing on Kapton sheets (0.005 inch thickness), the electrodes were cured in a box furnace at 350 °C for 30 min. The hBN ionogel was printed on top of the graphene electrodes using the same print settings as the graphene ink. Alignment between print layers was achieved through camera recognition of printed fiducial markers. Finally, the devices were placed on a hot plate at 160 °C for 30 min to remove sequestered EL solvent. All electrochemical testing was performed with a potentiostat (VSP, BioLogic). A detailed description of the formulas used for areal capacitance, energy density, and power density are reported in the Supporting Information. The entire footprint area of the device, including the gaps between electrode fingers, was considered for the area-normalized calculations.

High-Temperature Characterization: High-temperature device characterization was performed while the devices were taped to a hot plate at the specified temperature. Extended leads were painted on the substrate using silver paint so that the devices could be attached to the measurement probes away from the hot plate (Figure S12, Supporting Information).

PVA Gel Electrolyte: The PVA–H_3PO_4 gel electrolyte was formed by mixing 4.5 g of deionized water, 0.5 g of H_3PO_4 (85%, Sigma–Aldrich), and 0.3 g of PVA (M_W: 89 000–98 000, Sigma–Aldrich), followed by stirring for 2 h at 80 °C. Cyclic voltammograms of the polymer devices are shown in Figure S13 (Supporting Information).

Supporting Information

Supporting Information is available from the Wiley Online Library or from the author.

Acknowledgements

This work was supported by the U.S. Department of Commerce, National Institute of Standards and Technology (Award No. 70NANB19H005) as part of the Center for Hierarchical Materials Design (CHiMaD) in addition to the National Science Foundation MADE-PUBLIC Future Manufacturing Research Grant Program (Award No. CMMI-2037026). L.E.C. was further supported by the National Science Foundation Graduate Research Fellowship under Grant No. DGE-1842165. The authors acknowledge Alexander Saavedra for designing the files used to pattern the mesh screens for screen printing, Cory Thomas for assistance with the ionic conductivity measurements and VFT fitting, and Heather Kurtz for assistance with the EIS equivalent circuit fitting.

Conflict of Interest

The authors declare no conflict of interest.

Data Availability Statement

The data that support the findings of this study are available from the corresponding author upon reasonable request.

Keywords

2D materials, dielectrics, energy storage, ionic liquid gels, screen printing

Received: May 31, 2023
Revised: July 14, 2023
Published online: August 15, 2023

[1] Z. L. Wang, *Adv. Mater.* **2012**, *24*, 280.
[2] A. Khodabandehlo, A. Noori, M. S. Rahmanifar, M. F. El-Kady, R. B. Kaner, M. F. Mousavi, *Adv. Funct. Mater.* **2022**, *32*, 2204555.
[3] M. Beidaghi, Y. Gogotsi, *Energy Environ. Sci.* **2014**, *7*, 867.
[4] C. Lethien, J. L. Bideau, T. Brousse, *Energy Environ. Sci.* **2019**, *12*, 96.
[5] J. Hu, J. Luo, Z. Xu, K. Xie, H. Yu, H. Wang, C. Shen, L. H. Qi, B. Wei, *Appl. Phys. Rev.* **2021**, *8*, 011401.
[6] P. Simon, Y. Gogotsi, *Nat. Mater.* **2008**, *7*, 845.
[7] A. Noori, M. F. El-Kady, M. S. Rahmanifar, R. B. Kaner, M. F. Mousavi, *Chem. Soc. Rev.* **2019**, *48*, 1272.
[8] C. Wang, M. Muni, V. Strauss, A. Borenstein, X. Chang, A. Huang, S. Qu, K. Sung, T. Gilham, R. B. Kaner, *Small* **2021**, *17*, 2006875.
[9] C. Gao, J. Huang, Y. Xiao, G. Zhang, C. Dai, Z. Li, Y. Zhao, L. Jiang, L. Qu, *Nat. Commun.* **2021**, *12*, 2647.
[10] H. Li, J. Liang, *Adv. Mater.* **2020**, *32*, 1805864.
[11] B. D. Gates, *Science* **2009**, *323*, 1566.
[12] J. P. Mensing, T. Lomas, A. Tuantranont, *Sustainable Mater. Technol.* **2020**, *25*, e00190.
[13] L. J. Deiner, T. L. Reitz, *Adv. Energry Mater.* **2017**, *19*, 1600878.
[14] K. Suganuma, in *Introduction to Printed Electronics*, Springer, New York **2014**, pp. 1–22.
[15] G. Hu, J. Kang, L. W. T. T. Ng, X. Zhu, R. C. T. T. Howe, C. G. Jones, M. C. Hersam, T. Hasan, *Chem. Soc. Rev.* **2018**, *47*, 3265.
[16] X. Wang, G. Shi, *Energy Environ. Sci.* **2015**, *8*, 790.
[17] M. F. El-Kady, Y. Shao, R. B. Kaner, *Nat. Rev. Mater.* **2016**, *1*, 16033.
[18] L. Li, E. B. Secor, K. S. Chen, J. Zhu, X. Liu, T. Z. Gao, J. W. T. Seo, Y. Zhao, M. C. Hersam, *Adv. Energy Mater.* **2016**, *6*, 1600909.
[19] J. Li, F. Ye, S. Vaziri, M. Muhammed, M. C. Lemme, M. Östling, *Adv. Mater.* **2013**, *25*, 3985.
[20] A. G. Kelly, D. O'Suilleabhain, C. Gabbett, J. N. Coleman, *Nat. Rev. Mater.* **2022**, *7*, 217.
[21] E. Jabari, F. Ahmed, F. Liravi, E. B. Secor, L. Lin, E. Toyserkani, *2D Mater.* **2019**, *6*, 042004.
[22] J. Li, S. Sollami Delekta, P. Zhang, S. Yang, M. R. Lohe, X. Zhuang, X. Feng, M. Östling, *ACS Nano* **2017**, *11*, 8249.
[23] D. Jiang, H. Liang, W. Yang, Y. Liu, X. Cao, J. Zhang, C. Li, J. Liu, J. J. Gooding, *Carbon* **2019**, *146*, 557.
[24] L. Liu, Q. Tian, W. Yao, M. Li, Y. Li, W. Wu, *J. Power Sources* **2018**, *397*, 59.
[25] J. Liang, C. Jiang, W. Wu, *Appl. Phys. Rev.* **2021**, *8*, 021319.
[26] H. Zhang, Y. Qiao, Z. Lu, *ACS Appl. Mater. Interfaces* **2016**, *8*, 32317.
[27] J. Liang, Y. Feng, L. Liu, S. Li, C. Jiang, W. Wu, *J. Mater. Chem. A* **2019**, *7*, 15960.
[28] V. Rajendran, A. M. V. Mohan, M. Jayaraman, T. Nakagawa, *Nano Energy* **2019**, *65*, 104055.
[29] X. Shi, S. Pei, F. Zhou, W. Ren, H.-M. Cheng, Z.-S. Wu, X. Bao, *Energy Environ. Sci.* **2019**, *12*, 1534.
[30] S. Fletcher, V. Black, US9318271B2, **2016**.
[31] R. S. Borges, A. L. M. Reddy, M. T. F. Rodrigues, H. Gullapalli, K. Balakrishnan, G. G. Silva, P. M. Ajayan, *Sci. Rep.* **2013**, *3*, 2572.
[32] J. Watson, G. Castro, *J. Mater. Sci.* **2015**, *26*, 9226.
[33] R. W. Johnson, *Adv. Packag.* **2004**, *13*, 40.
[34] X. J. Liu, M. S. Zheng, G. Chen, Z. M. Dang, J. W. Zha, *Energy Environ. Sci.* **2022**, *15*, 56.
[35] W. J. Hyun, L. E. Chaney, J. R. Downing, A. C. M. de Moraes, M. C. Hersam, *Faraday Discuss.* **2021**, *227*, 92.
[36] W. J. Hyun, C. M. Thomas, L. E. Chaney, A. C. Mazarin de Moraes, M. C. Hersam, *Nano Lett.* **2022**, *22*, 5372.
[37] W. J. Hyun, C. M. Thomas, M. C. Hersam, *Adv. Energy Mater.* **2020**, *10*, 2002135.
[38] W. J. Hyun, A. C. M. de Moraes, J.-M. Lim, J. R. Downing, K.-Y. Park, M. T. Z. Tan, M. C. Hersam, *ACS Nano* **2019**, *13*, 9664.

[39] T. S. Tran, N. K. Dutta, N. R. Choudhury, *Adv. Colloid Interface Sci.* **2018**, *261*, 41.
[40] S. Alipoori, S. Mazinani, S. H. Aboutalebi, F. Sharif, *J. Energy Storage* **2020**, *27*, 101072.
[41] Q. Chen, X. Li, X. Zang, Y. Cao, Y. He, P. Li, K. Wang, J. Wei, D. Wu, H. Zhu, *RSC Adv.* **2014**, *4*, 36253.
[42] W. J. Hyun, E. B. Secor, M. C. Hersam, C. D. Frisbie, L. F. Francis, *Adv. Mater.* **2015**, *27*, 109.
[43] N. Liu, Y. Gao, *Small* **2017**, *13*, 1701989.
[44] L. Wang, H. Yao, F. Chi, J. Yan, H. Cheng, Y. Li, L. Jiang, L. Qu, *ACS Nano* **2022**, *16*, 12813.
[45] N. A. Kyerematen, T. Brousse, D. Pech, *Nat. Nanotechnol.* **2017**, *12*, 7.
[46] H. Sun, X. Fu, S. Xie, Y. Jiang, H. Peng, *Adv. Mater.* **2016**, *28*, 2070.
[47] Y. Cui, Y. Xie, Y. Wu, H. Ma, Z. Zhou, Q. Huang, J. Ye, **2018**, *10*, 26357.
[48] S. K. Kim, H. J. Kim, J. C. Lee, P. V. Braun, H. S. Park, *ACS Nano* **2015**, *9*, 8569.
[49] B. Asbani, C. Douard, T. Brousse, J. L. Bideau, *Energy Storage Mater.* **2019**, *21*, 439.
[50] B. Shen, R. Guo, J. Lang, L. Liu, L. Liu, X. Yan, *J. Mater. Chem. A* **2016**, *4*, 8316.
[51] T. Mao, S. Wang, X. Wang, F. Liu, J. Li, H. Chen, D. Wang, G. Liu, J. Xu, Z. Wang, *ACS Appl. Mater. Interfaces* **2019**, *11*, 17742.
[52] K. Park, J. Lim, N. S. Luu, J. R. Downing, S. G. Wallace, L. E. Chaney, H. Yoo, W. J. Hyun, H. Kim, M. C. Hersam, *Adv. Energy Mater.* **2020**, *10*, 2001216.